In vivo Dosimetry Using MOSFET dosimeters in External Beam Radiation Therapy

Tetsuzo Nara, Kazuhiko Sato, Fumio Komai,
Hideto Fukusi, Yosiaki Horanai, Sadao Watanabe,
Akira Iwasaki[1)]

Department of Radiation Oncology, Aomori Prefectural Central Hospital
1) School of Medicine, Department of Health Science, Former Hirosaki University

Keywords: MOSFET dosimeter, In vivo dosimetry, Collision kerma, Quality Assurance, External Beam Radiation Therapy

Abstract

In performing in vivo dosimetry using MOSFET dosimeters, we first evaluated the performance of the MOSFET dosimeter for 10 MV X-ray. The calibration factor and the coefficient of variation of angle dependence were 3.0% and 3.4%, respectively, at maximum. The coefficient of determination, R^2, exhibited high goodness of fit index linearity at 0.9996 or higher. The TMR in the 20-cm-thick laminated solid tough water phantom measured by MOSFET dosimeters at a depth ranging from 1 cm to 19 cm exhibited a relative error of -4% or less relative to the TMR measured in the semi-infinite phantom with the 0.13 cm^3 ionization chamber**.** At a depth of 20 cm on the surface on the exit side, the relative error of mean dose of two MOSFET dosimeters was -6.8% as a result of build-down effect due to shortage of backscatter factor.

Second, comparison of the accuracy of target dose estimation of isocenter by in vivo dosimetry from exit side of MOSFET dosimeter estimated from the mean dose of two MOSFET dosimeters between the 20-cm-thick laminated solid tough water phantom and the oval water equivalent phantom revealed that the maximum relative error was -2.8% in the former and -6.1% in the latter.

Introduction

The dose to be administered to the target volume in external beam radiation therapy is determined according to the value of monitor unit (MU) obtained from treatment planning system (TPS) and the manual calculation. The target dose actually exposed is usually verified based on this MU value by applying the dose to a solid phantom or water phantom with the same irradiation technique. This method, however, enables verification only on a phantom, with effects of body movement (including movement of the heart, breathing, the gastrointestinal tract, and so on) and changes in body thickness during the period between treatment planning for patients and actual delivery of irradiation, which are likely in practical treatment, not reflected in it. In total body irradiation (TBI), which is external beam radiation therapy performed before bone marrow transplantation, in vivo dosimetry[1-3)] is performed for each irradiation. Since this radiotherapy is performed several times, if the measured dose does not match the target dose, the dose can be adjusted before completion of treatment. In vivo dosimetry has the advantage of enabling checking for miscalculation of the MU value and unforeseen changes in energy output caused by the accelerator by evaluation of the target dose in general external beam radiation therapy as well. This advantage is believed to contribute to quality assurance (QA) in radiotherapy. We have developed a method of estimating target dose by in vivo dosimetry with attached two MOSFET dosimeters [4-7)], which are compact and capable of being easily attached to the cutaneous surface of patients and of measuring doses in real time, to the exit side of the X-ray. We will report on this method.

1. Theory

1-1 Method of estimating target dose (D_T) from surface dose on the exit side (D_E)

Fig. 1 (a) is a conceptual rendering of the relationship between the placement of a MOSFET dosimeter and position of the isocenter based on a fixed one-field irradiation

source with a constant source-to-axis distance (SAD). The phantoms used are all water equivalent. Fig. 1 (b) is an explanatory diagram for Fig. 1 (a). The target dose is expressed as D_T and the surface dose on the exit side as D_E in Fig. 1 (b). In addition, the irradiation fields at the respective doses are expressed as A_T and A_E. The surface of the exit side of the finite-thickness phantom (Fig. 1 (b)) is a build-down area[3]. Fig. 1 (c) explains compensation for dose shortage resulting from decreased D_E due to insufficient backscatter. Fig. 1 (d) shows the dose (D_0, D'_0) and the in-air water collision kerma (K_1, K_2) at the maximum depth (d_{max}) corresponding to the positions of doses D_T and D_E.

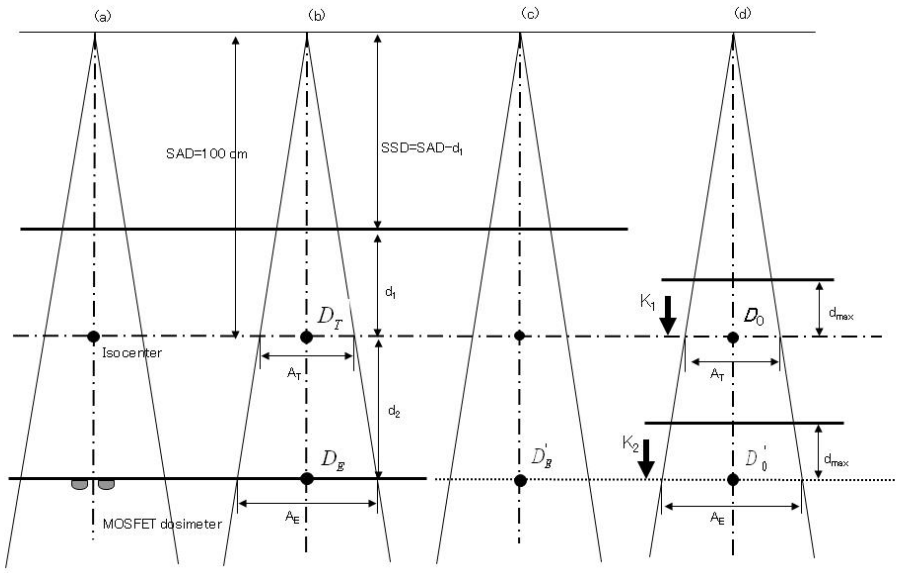

Fig. 1 A conceptual rendering showing calculation of the target dose in the isocenter from the MOSFET dose value on the surface of exit side. (a) shows a layout plan for MOSFET dosimeters in a water equivalent phantom. (b) shows a geometric layout of water equivalent phantom. D_E is the surface dose on the exit side and D_T the target dose at the isocenter position. (c) shows the geometric layout in the semi-infinite phantom. D'_E shows the dose in a semi-infinite phantom corresponding to the surface dose on the exit side (D_E). (d) shows the maximum depth doses, D_0 and D'_0, which correspond to D_T and D'_E , respectively. K_1 and K_2 refer to in-air water collision kermas corresponding to D_0 and D'_0, respectively.

A method of obtaining D_T at the isocenter from the D_E at the surface of the exit side is shown below. In the following equation, TMR (d, A) is the tissue maximum ratio (TMR) at depth d in the irradiation field A.

From Fig. 1 (b) and Fig. 1 (d), D_T is expressed in the following equation.

$$D_T = \mathrm{TMR}(d_1, A_T) \times D_0$$
$$= \mathrm{TMR}(d_1, A_T) \times f \times K_1 \times S_p(A_T) \cdots (1)$$

where D_0 is the dose at the maximum depth (d_{max}), f is a constant, K_1 is the in-air water collision kerma against D_0, and S_p (A_T) is the phantom scattering coefficient in the irradiation field (A_T). (refer to Appendix A)

Second, we discuss D_E and D'_E as shown in Fig. 1 (b) and Fig. 1 (c). The relationship between dose D_E in the finite-thickness phantom shown in Fig. 1 (b) and the dose D'_E in the semi-infinite phantom in the same positional relations as D_E indicated in Fig. 1 (c) is shown below. The full backscatter factor (BSF) is expressed in the following equation.

$$\text{BSF}(A_E) = \frac{D'_E(A_E)}{D_E(A_E)} \quad \cdots\cdots(2)$$

where BSF (A_E) is the saturated backscatter factor in the irradiation field (A_E). BSF is a function of the irradiation field. BSF (A_E) is evaluated based on the MOSFET dosimeter readings on the surface of the exit side of the finite-thickness phantom and in backscatterers with various thicknesses.

The relationship between D'_E and D'_0 in Fig. 1 (c) and Fig. 1 (d) is expressed below:

$$D'_E = \text{TMR}(d_1 + d_2, A_E) \times D'_0 \cdots(3)$$

Furthermore, with reference to Appendix A, the above equation can be converted to:

$$D'_E = \text{TMR}(d_1 + d_2, A_E) \times f \times K_2 \times S_p(A_E) \cdots(4)$$

where D'_0 is the dose at the maximum depth (d_{max}) and K_2 is the in-air water collision kerma for D'_0. Therefore, from Equations (2) and (3), the following equation is obtained:

$$D_E = \frac{\text{TMR}(d_1+d_2, A_E) \times f \times K_2 \times S_p(A_E)}{\text{BSF}(A_E)} \cdots(5)$$

where S_p (A_E) is the phantom scatter factor in the irradiation field A_E. In addition, the relationship between the two in-air water collision kermas, K_1 and K_2, is expressed as:

$$\frac{K_1}{K_2} = \left(\frac{SAD + d_2}{SAD}\right)^2 \cdots\cdots(6)$$

D_T obtained from D_E is as follows by Equations (1), (5), and (6):

$$D_T = \left(\frac{\mathrm{SAD}+d2}{SAD}\right)^2 \times \frac{\mathrm{TMR}(d_1, A_T)\times S_P(A_T)}{\mathrm{TMR}(d_1+d_2, A_E)\times S_P(A_E)}$$
$$\times D_E \times \mathrm{BSF}\,(A_E) \quad (7)$$

1-2 Calibration factor for the MOSFET dosimeter and dose D_T based on the calibration factor

The ratio of the absorbed dose (cGy) to the MOSFET dosimeter reading at a given underwater point (mV), (cGy/mV), will be defined as a calibration factor (CF). If the MOSFET dosimeter reading on the surface of the exit side against D_E in Equation (7) is M_E, Equation (7) becomes:

$$D_T = \left(\frac{\mathrm{SAD}+d2}{\mathrm{SAD}}\right)^2 \times \frac{\mathrm{TMR}(d_1, A_T)\times S_P(A_T)}{\mathrm{TMR}(d_1+d_2, A_E)\times S_P(A_E)}$$
$$\times \mathrm{BSF}(A_E)\times M_E \times \mathrm{CF} \quad (8)$$

2. Devices used and experimental method

2-1 MOSFET dosimetry system

The MOSFET dose calculation system (Thomson & Nielsen) consists of the Reader Module (TN-RD-16) and the MOSFET dosimeters. One unit of the Reader Module can be connected to up to five MOSFET dosimeters. The standard size of a MOSFET dosimeter (Standard TN-502RD) is 0.2 cm in width × 0.8 cm in length × 0.13 cm in thickness (effective detection area: 0.02 ×0.02 cm^2, specific build-up thickness: 0.08 cm). The projecting side of the detecting element of the MOSFET dosimeter is called the epoxy side while the opposite flat side is termed the flat side [7]. The bias voltage used in the experiment was the standard value of 9 V, at which the maximum reading was saturated at 20000 mV.

2-2 Devices and instruments used

The experiment used a medical linear accelerator generating 10 MV X-ray (EXL-20DP: Mitsubishi Electric Corporation).

For comparison with MOSFET dosimeters, a 0.13 cm^3 thimble (Type-CC13, Advanced 3D water phantom system, Scanditronix, Wellhofer) and 0.6 cm^3 thimble (Type-TM30006, electrometer UNIDOS, PTW) ionization chambers were used.

Phantoms selected for the experiment were a 16 cm φ cylindrical water equivalent phantom (Model-002HN, CIRS), an oval water equivalent phantom (30 cm in width × 20 cm in height, Model-002H5, CIRS), and a laminated solid tough water phantom (surface area 30 × 30 cm^2, Kyoto Kagaku).

2-3 Evaluation of performance and accuracy of target dose estimation for MOSFET dosimeters

First, the performance of the MOSFET dosimeters with 10 MV X-ray was evaluated. Seven parameters of evaluation were selected: (1) CF, (2) linearity, (3) angle dependence, (4) TMR of the finite-thickness phantom, and (5) BSF, as items for evaluation of

performance, and (6) the laminated solid tough water phantom and (7) the oval water equivalent phantom as items of evaluation for accuracy of target dose estimation by in vivo dosimetry. Not all of the above items can be evaluated by a single MOSFET dosimeter since reading is saturated at 20000 mV. Table 1 shows the parameters of evaluation of performance corresponding to the serial numbers of the individual MOSFET dosimeters.

							laminated solid tough water phantom	oval water equivaler phantom
Number	Serial No	CF	Linearity	Angular dependence	TMR	BSF	In vivo dosimetry	In vivo dosimetr
MOSFET 1	SN14003	○				○	○	○
MOSFET 2	SN16060	○				○	○	○
MOSFET 3	SN16062	○	○			○		
MOSFET 4	SN16063	○	○	○		○		
MOSFET 5	SN17039	○		○	○	○		
MOSFET 6	SN17040	○			○	○		

Table 1. Items of evaluation of performance for MOSFET dosimeters

2-3-1 CFs for MOSFET dosimeters

MOSFET dosimetry was performed with the six MOSFET dosimeters No. 1 to No. 6, by irradiating the 20-cm-thick laminated solid tough water phantom so that the prescribed dose was 100 cGy at a depth of 10 cm in a fixed one-field radiation for 10×10 cm^2 of irradiation field at a source-to-chamber distance (SCD) of 100 cm. Measurements were made with the MOSFET dosimeters in pairs 20 times.

2-3-2 Linearity of MOSFET dosimeters

MOSFET dosimetry was performed by irradiating the 20-cm-thick laminated solid tough water phantom at a depth of 10 cm (SCD 100 cm) with the flat side faced toward the radiation source and with MOSFET dosimeters No. 3 and No. 4 aligned at the same time. The dose rate of the linear accelerator was set constant at 300 (MU/min) with irradiation field of 10 × 10 cm^2, as usually used for clinical treatment. The doses administered at a depth of 10 cm were 20, 50, 100, 150, 200, and 300 (cGy).

2-3-3 Angle dependence of MOSFET dosimeters

MOSFET dosimetry was performed by placing MOSFET dosimeters No. 4 and No. 5 one by one on the center of the 16 cm φ cylindrical water equivalent phantom (at 8 cm in depth, SCD 100 cm) with the epoxy side directed at 0 degree gantry rotation angle of the linear accelerator. The angle of the MOSFET dosimeter in the above conditions was defined as 0 degrees and the reading (mV) as 100. Dosimetry was performed at angles ranging from 0 to 330 degrees with the MOSFET dosimeter rotated at each 30-degree increments relative to a 0 degree gantry rotation angle of the linear accelerator. The MU value was set constant at 100 in a irradiation field of 10 × 10 cm^2.

2-3-4 TMR of the finite-thickness laminated solid tough water phantom obtained by MOSFET dosimeter

MOSFET dosimetry was performed in the 20-cm-thick laminated solid tough water phantom with two MOSFET dosimeters No. 5 and No. 6 with the MU value set constant at 100 in a irradiation field of 10 × 10 cm^2. Dosimetry was performed three times by simultaneously placing the two dosimeters at the same depth, and the respective mean TMRs of the dosimeters were normalized to the value at a depth of 2.5 cm. Since the dose will decrease in TMR measurement in the 20-cm-thick laminated solid tough water phantom at 20 cm in depth (the surface of the exit side) as the position approaches the exit side due to the build-down area[3)], the corresponding TMRs were compared with TMRs obtained in the 3D water phantom system mounted with the 0.13 cm^3 ionization chamber.

2-3-5 BSFs obtained by MOSFET dosimeters

BSFs were obtained from Equation (2) using MOSFET dosimeters (1) to (6) after upward irradiation with the MU value set constant at 100 and with the gantry rotation angle of the linear accelerator set at 180 degrees. Irradiation was performed in four types of irradiation fields: 5×5 cm^2, 10×10 cm^2, 15×15 cm^2, and 20×20 cm^2. The MOSFET dosimeters were placed on the 10 cm-thick (SCD 100 cm) laminated solid tough water phantom with the flat side faced to the radiation source. In the respective irradiation fields, phantoms were stacked from 0 cm to 30 cm in thickness on the MOSFET dosimeters one after another. The BSFs measured were compared with BSFs obtained with the 0.6 cm^3 ionization chamber.

2-3-6 Accuracy of target dose estimation in in vivo dosimetry with laminated solid tough water phantom

Figs. 2 (a) to (c) show in vivo dosimetry layouts of the 20-cm-thick laminated solid tough water phantom. Figs. (a) to (c) are layouts of the phantom with isocenter depths of 4 cm, 10 cm, and 16 cm (SCD 100 cm), respectively. MOSFET dosimetry was performed for the surface dose on the exit side with MOSFET dosimeters No. 1 and 2 placed at the same time with the flat side faced to the radiation source at 0-degree gantry rotation angle of the linear accelerator. Dosimetry was performed with the MU value set constant at 100 in three types of irradiation fields: 5×5 cm^2, 10×10 cm^2, and 20×20 cm^2, for the respective isocenters. The target dose in the isocenter was estimated from the surface dose on the exit side using Equation (8). In addition, the target dose in the isocenter was compared with the value measured with the 0.6 cm^3 ionization chamber.

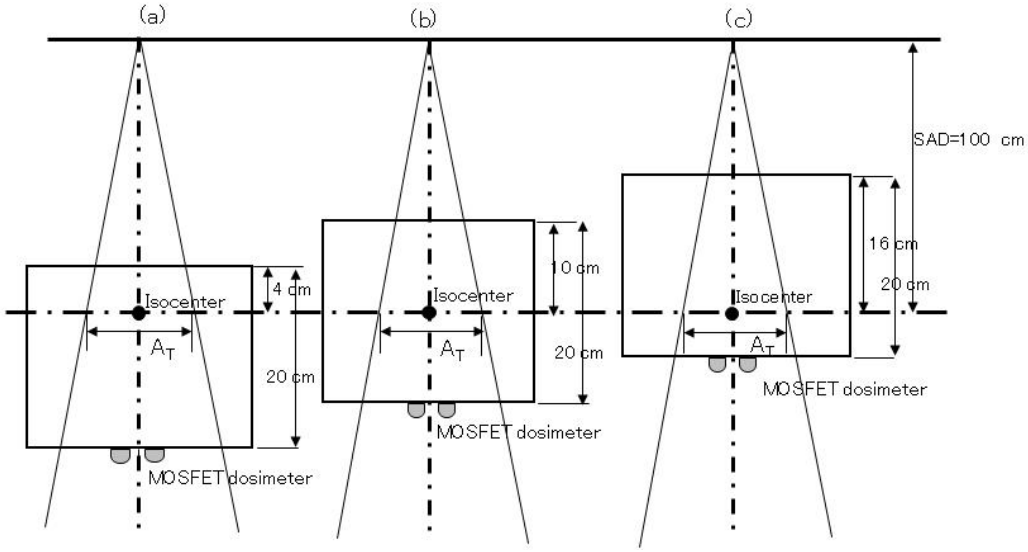

Fig. 2 A dosimetry layout plan for estimating target dose at the isocenter using the 20-cm-thick laminated solid tough water phantom. Figs. (a) to (c) show the layout plans at isocenter depths of 4 cm, 10 cm, and 16 cm, respectively.

2-3-7 Accuracy of target dose estimation in in vivo dosimetry in oval water equivalent phantom

Fig. 3 shows a layout plan for in vivo dosimetry performed in the oval water equivalent phantom with MOSFET dosimeters No. 1 and No. 2 attached to the surface of exit side with their flat sides faced toward the radiation source. Dosimetry was performed in three types of irradiation fields: 5×5 cm^2, 10×10 cm^2, and 20×20 cm^2, at gantry angles of the linear accelerator ranging from 0 to 330 degrees at 30 degrees interval (at 0 degrees, 30 degrees, and 330 degrees, the two MOSFET dosimeters were directly attached to the mylar sheet). The target dose at isocenter was estimated from the surface dose on the exit side using Equation (8). The dose delivered at the isocenter was 100 (cGy).

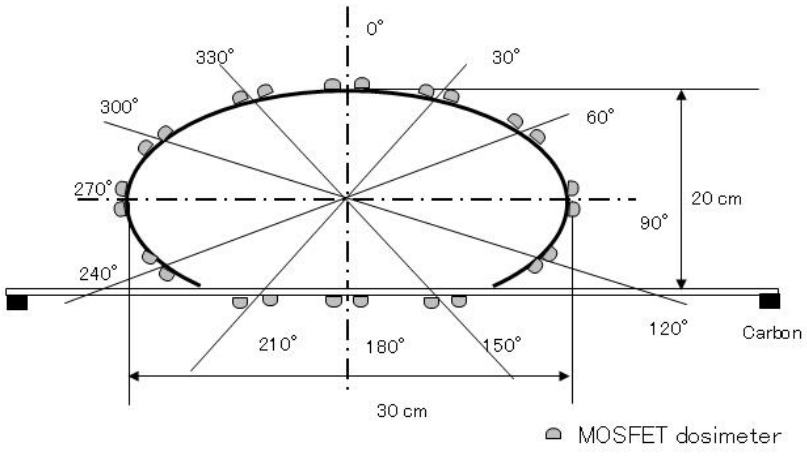

Fig. 3 A dosimetry layout plan for estimating target dose at the isocenter using the oval water equivalent phantom**.** Measurement was performed at each 30 degrees intervals of gantry rotation angle.

3. Results

3-1 CFs obtained by MOSFET dosimeters

Fig. 4 shows the CFs obtained using the MOSFET dosimeters No. 1 to No. 6, in the order of serial numbers. The horizontal axis of the figure indicates the number of measurement and the vertical axis the CF. In Fig. 4, □ indicates MOSFET dosimeter No. 1, ▲ MOSFET dosimeter No. 2, × MOSFET dosimeter No. 3, ■ MOSFET dosimeter No. 4, ◇ MOSFET dosimeter No. 5, and △ MOSFET dosimeter No. 6. The respective figures are shown in line charts. The mean values of CFs for MOSFET dosimeters ranged from 0.8873 to 0.9062, the standard deviation (σ) ranged from 0.012 to 0.027, and the coefficient of variation (CV) ranged from approximately 1.4% to 3.0%.

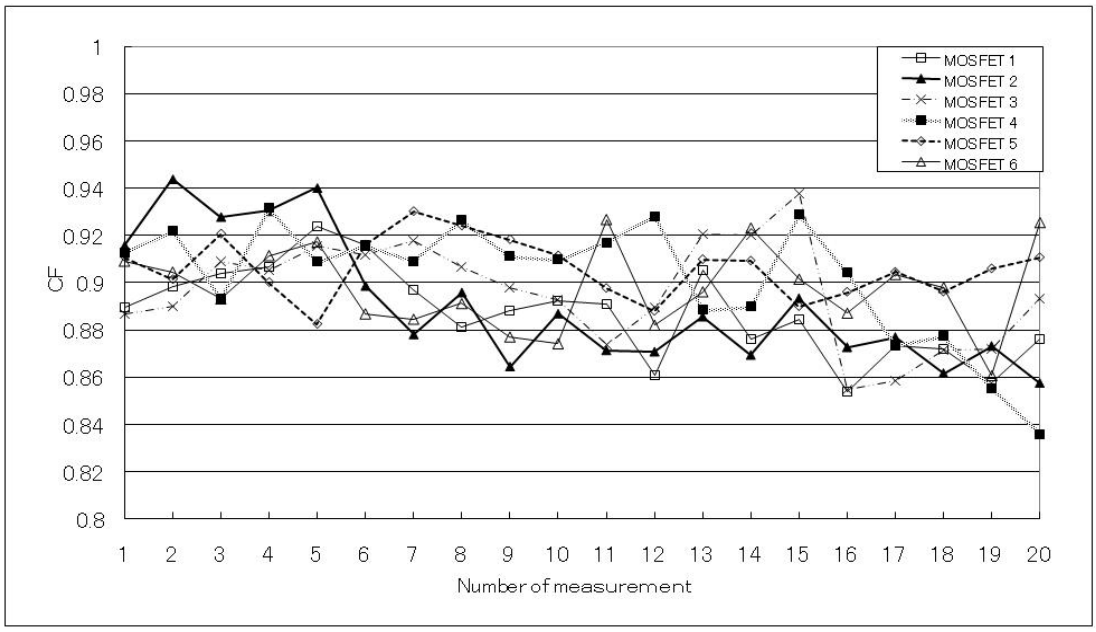

Fig. 4 Figure showing changes in calibration factor (CF) for each MOSFET dosimeter number.

3-2 Linearity of MOSFET dosimeters

Fig. 5 shows the linearity of MOSFET dosimeters No. 3 and No. 4. The horizontal axis in the figure indicates the dose and the vertical axis the reading of the MOSFET dosimeter (mV). In Fig. 5, X indicates the measurement for MOSFET dosimeter No. 3 and ■ the measurement for MOSFET dosimeter No. 4. The dotted line connects the respective values for MOSFET dosimeter No. 3, and the solid line was plotted from the respective values for MOSFET dosimeter No. 4. The coefficient of determination for the linear approximate equation, R^2, was 0.9996 or higher.

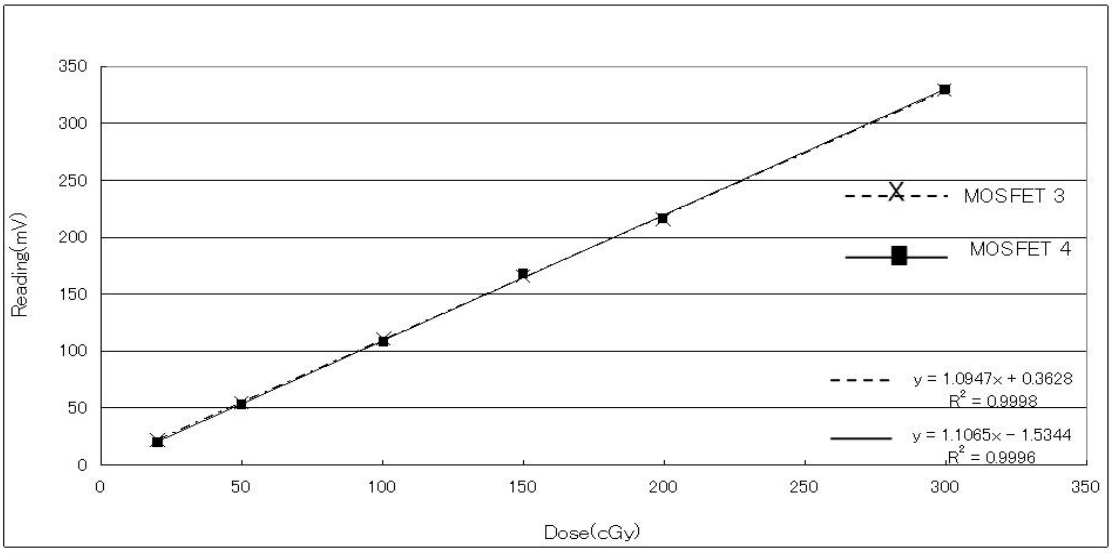

Fig. 5 Figure showing linearity of MOSFET dosimeter No. 3 and MOSFET dosimeter No. 4.

3-3 Angle dependence of MOSFET dosimeters

Fig. 6 shows the mean angle dependence values measured for MOSFET dosimeters No. 4 and No. 5 at the same angle three times. The horizontal axis in the figure indicates the rotation angle of the MOSFET dosimeters and the vertical axis the relative sensitivity of the MOSFET dosimeters, with the value for the MOSFET dosimeters with the epoxy side directed at 0-degree gantry rotation angle defined as 100. In Fig. 6, ■ indicates the result for MOSFET dosimeter No. 4 and ◇ the result for MOSFET dosimeter No. 5. The relative sensitivity of MOSFET dosimeter No. 4 at 30 degrees was 102.24 ± 2.12%. The relative sensitivity of MOSFET dosimeter No. 5 at 90 degrees was 96.37 ± 2.98%.

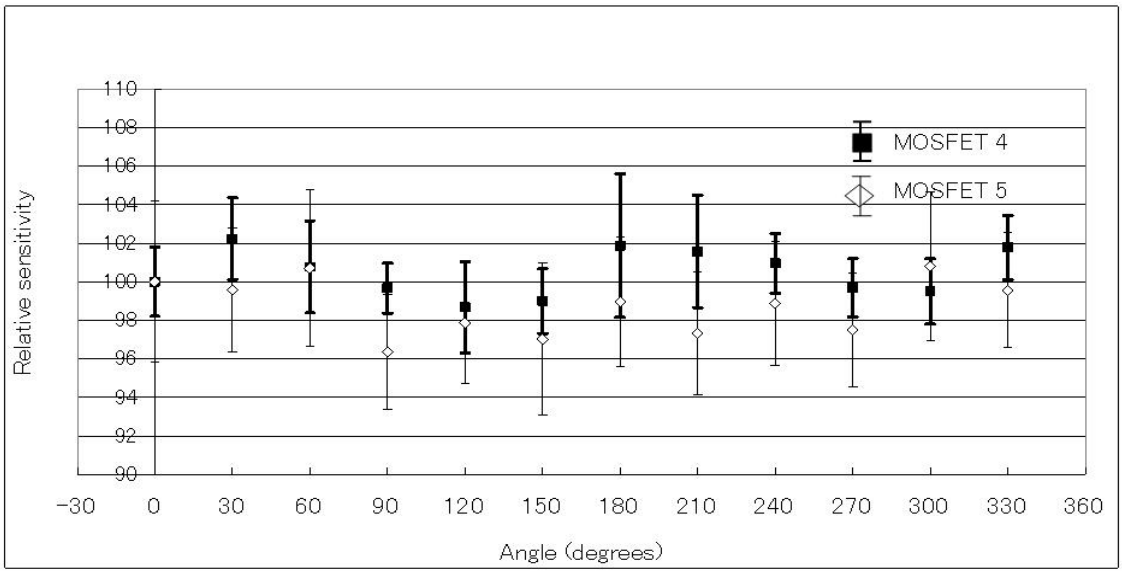

Fig. 6 Figure showing angle dependence of MOSFET dosimeters No. 4 and No. 5 for 10 MV X-irradiation. The target phantom is a 16 cm φ cylindrical water equivalent phantom.

3-4 TMR of the laminated solid tough water phantom obtained by MOSFET dosimeter

Fig. 7 shows TMR values measured for MOSFET dosimeters No. 5 and No. 6 in the 20-cm-thick laminated solid tough water phantom and TMR values measured in the 3D water phantom system mounted with the 0.13 cm^3 ionization chamber. In the figure, the horizontal axis indicates the depth (cm) and the vertical axis the TMR. In Fig. 7, ◇ indicates the TMR of MOSFET dosimeter No. 5, △ the TMR of MOSFET dosimeter No. 6, and the solid line the TMR of the 0.13 cm^3 ionization chamber. The maximum relative errors of the TMRs measured for MOSFET dosimeters No. 5 and No. 6 at a depth of 1 cm to 19 cm against the TMR measured for the 0.13 cm^3 ionization chamber were -4% and -3% or less, respectively. On the surface of the exit side at a depth of 20 cm, TMRs decreased for both MOSFET dosimeters. Standard deviations for both MOSFET dosimeters are also out of range.

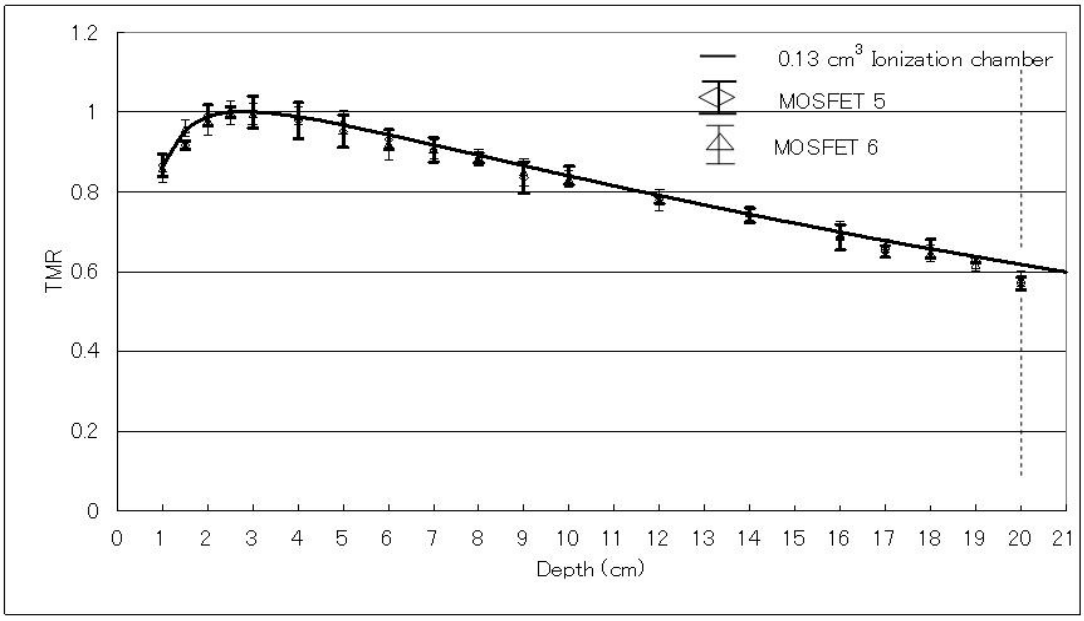

Fig. 7. Figure showing TMR measured in the 20-cm-thick laminated solid tough water phantom by MOSFET dosimeters in a irradiation field of 10 × 10 cm^2. The dosimeters were normalized to the value at a reference depth 2.5 cm. ◇ indicates MOSFET dosimeter No. 5, △ MOSFET No. 6, and the solid line the TMR measured in the semi-infinite 3D water phantom system with the 0.13 cm^3 ionization chamber.

3-5 BSF obtained by MOSFET dosimeters

Fig. 8 shows the BSF measured for MOSFET dosimeters No. 1 to No. 6 and the 0.6 cm^3 ionization chamber. In the figure, the horizontal axis indicates the irradiation field and the vertical axis the BSF. In Fig. 8, □ indicates MOSFET dosimeter No. 1, ▲ MOSFET dosimeter No. 2, × MOSFET dosimeter No. 3, ■ MOSFET dosimeter No. 4, ◇ MOSFET dosimeter No. 5, and △ MOSFET dosimeter No. 6. In addition, ● indicates the result of measurement for the 0.6 cm^3 ionization chamber. The curved lines were simply plotted from the respective values measured for the dosimeters. The MOSFET dosimeters yielded lower values than that for the 0.6 cm^3 ionization chamber.

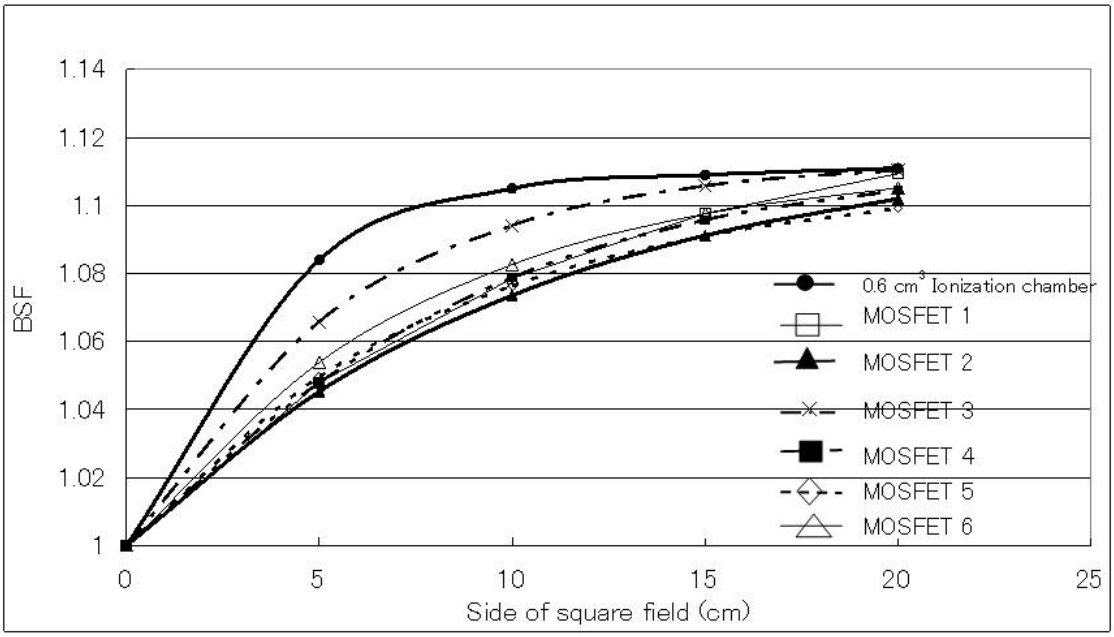

Fig. 8 Changes in saturated full backscatter factor (BSF) in a square irradiation field. □, ▲, ×, ■, ◇, and △ marks indicate results for MOSFET dosimeters with serial number. ● indicates the result of measurement with the 0.6cm^3 ionization chamber.

3-6 Accuracy of target dose estimation in in vivo dosimetry with laminated solid tough water phantom

Tables 2 (1) to (3) show the results for target doses in the isocenter estimated according to Equation (8) using the dose on the surface of exit side of MOSFET dosimeters No. 1 and No. 2 attached to the surface of the exit side of the 20-cm-thick laminated solid tough water phantom. Tables 2 (1) to (3) show the target doses in the isocenter directly measured with the 0.6 cm^3 ionization chamber, the respective estimated doses for MOSFET dosimeters No. 1 and No. 2, and their mean values. In addition, the tables show the relative errors of the values for MOSFET dosimeters No. 1 and No. 2 and their mean doses against the dose measured with the 0.6 cm^3 ionization chamber.

(1) Isocenter depth 4 cm

Field(cm^2)	0.6 cm^3 Thimble ionization chamber	MOSFET 1 (cGy)	%Error	MOSFET 2 (cGy)	%Error	MOSFET 1&2 Mean (cGy)	%Error
5 × 5	93.0	95.8	3.01	93.8	0.86	94.8	1.94
10 × 10	98.7	99.9	1.22	97.5	−1.22	98.7	0.00
20 × 20	103.2	99.8	−3.29	101.6	−1.55	100.7	−2.42

(2) Isocenter depth 10 cm

Field(cm^2)	0.6 cm^3 Thimble ionization chamber	MOSFET 1 (cGy)	%Error	MOSFET 2 (cGy)	%Error	MOSFET 1&2 Mean (cGy)	%Error
5 × 5	77.3	75.4	−2.46	75.6	−2.20	75.5	−2.33
10 × 10	84.9	80.9	−4.71	84.2	−0.82	82.6	−2.77
20 × 20	91.1	92.5	1.54	93.9	3.07	93.2	2.31

(3) Isocenter depth 16 cm

Field(cm^2)	0.6 cm^3 Thimble ionization chamber	MOSFET 1 (cGy)	%Error	MOSFET 2 (cGy)	%Error	MOSFET 1&2 Mean (cGy)	%Error
5 × 5	63.1	63.2	0.16	59.6	−5.55	61.4	−2.69
10 × 10	70.9	71.0	0.14	71.4	0.71	71.2	0.42
20 × 20	78.3	78.7	0.51	79.9	2.04	79.3	1.28

Table 2. Accuracy of target dose estimation in the isocenter using the 20-cm-thick laminated solid tough water phantom. Tables (1) to (3) show measurements and estimated values at isocenter depths of 4 cm, 10 cm, and 16 cm, respectively.

Table 2 (1) shows the results at an isocenter depth of 4 cm. The maximum relative error of MOSFET dosimeter No. 1 in the irradiation field of 20 × 20 cm^2 was -3.3% in Table 2 (1). The maximum relative error of the mean dose in the irradiation field of 20 × 20 cm^2 was -2.4%.

Table 2 (2) shows the results at an isocenter depth of 10 cm. The maximum relative error of MOSFET dosimeter No. 1 in the irradiation field of 10 × 10 cm^2 was -4.7% in Table 2 (2). The maximum relative error of the mean dose in the irradiation field of 10 × 10 cm^2 was -2.8%.

Table 2 (3) shows the results at an isocenter depth of 16 cm. The maximum relative error of the MOSFET dosimeter No. 2 in the irradiation field of 5 × 5 cm^2 was -5.5%. The maximum relative error of the mean dose in the irradiation field of 5 × 5 cm^2 was -2.7%.

3-7 Accuracy of target dose estimation in in vivo dosimetry in oval water equivalent phantom

Fig. 9 shows the accuracies of target dose estimation obtained with in vivo dosimetry using MOSFET dosimeters No. 1 and No. 2 attached on the surface of the exit side of the oval water equivalent phantom. The horizontal axis in the line chart of the

figure indicates the gantry rotation angle of the linear accelerator, and the vertical axis the relative error of the mean dose estimated from the MOSFET dosimeters No. 1 and No. 2 relative to the dose delivered at the isocenter, 100 (cGy). ◆ indicates the irradiation field of 5 × 5 cm^2, ▲ the irradiation field of 10 × 10 cm^2, and ■ the irradiation field of 20 × 20 cm^2. In the irradiation field of 5 × 5 cm^2, the maximum relative error -6.1% was observed at a gantry rotation angle of the linear accelerator of 30 degrees. In the irradiation field of 10 × 10 cm^2, the maximum relative error -4.3% was observed at a gantry rotation angle of 240 degrees. In the irradiation field of 20 × 20 cm^2, the maximum relative error +5.2% was observed at a gantry rotation angle of 60 degrees.

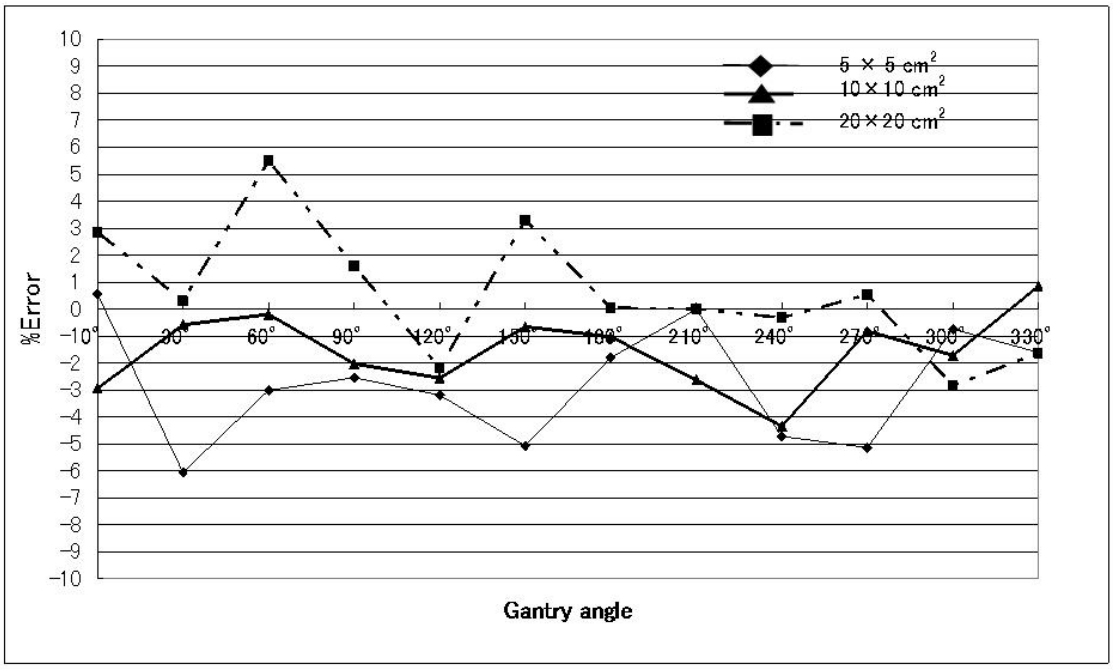

Fig. 9 Figure showing relative errors in target dose estimation relative to the gantry rotation angle in the oval water equivalent phantom. The fine line in the line chart indicates the irradiation field of 5 × 5 cm^2, the bold solid line the irradiation field of 10 × 10 cm^2, and the chain double-dashed line the irradiation field of 20 × 20 cm^2.

4. Discussion

Evaluation of the performance of the MOSFET dosimeter for 10 MV X-ray revealed that the coefficient of variation of CF in Item (1) for MOSFET dosimeter No. 5 was approximately 1.4% while that for MOSFET dosimeter No. 2 was approximately 3.0%. This difference in the results of two dosimeters was significant. Second, in terms of linearity in Item (2), the coefficients of determination, R^2, of MOSFET dosimeters No. 3 and No. 4 were showed high goodness of fit index at 0.9996 or higher. In terms of angle dependence in Item (3), the maximum coefficients of variation for MOSFET dosimeters No. 4 and No. 5 were approximately 3.4% and 2.8%, respectively. In terms of TMRs in Item (4), MOSFET dosimeters No. 5 and No. 6 exhibited relative errors of -4.0% and -3.0% or less, respectively, at a depth of 1 to 19 cm of the 20-cm-thick laminated solid tough water phantom. At a depth of 20 cm on the surface of the exit side, with a build-

down area generated due to insufficient backscatter due to air layer in the rear area, the relative errors of MOSFET dosimeters No. 5 and No. 6 in TMR against the value measured with 0.13 cm^3 ionization chamber for the semi-infinite phantom were -5.8% and -7.8%, respectively. The figure indicates that the build-down area may originate in an area approximately 1 cm inside the surface of the exit side (see Fig. 7).

In terms of accuracy of target dose estimation in the isocenter based on in vivo dosimetry with the 20-cm-thick laminated solid tough water phantom, the maximum relative error of the mean dose of MOSFET dosimeters No. 1 and No. 2 in the irradiation field of 10 × 10 cm^2 at an isocenter depth of 10 cm was -2.8%. The above finding indicates that the target dose can be estimated from in vivo dosimetry on the surface of the exit side even if the size of the irradiation field or the isocenter depth changes (see Table 2(2)). In terms of accuracy of target dose estimation based on in vivo dosimetry in the oval water equivalent phantom, the maximum relative error of the mean dose of MOSFET dosimeters No. 1 and No. 2 in the irradiation field of 5 × 5 cm^2 at a gantry rotation angle of 30 degrees was -6.1% (see Fig. 9). This finding indicates that in vivo dosimetry in the oval water equivalent phantom is less accurate compared with the results of the laminated solid tough water phantom, which may be partly as a result of angle dependence.

Accurate estimation of the target dose from in vivo dosimetry using the MOSFET dosimeter attached to the surface of the exit side could be obtained by compensating the insufficient backscatter on the exit side. In the vicinity of the surface on the exit side, however, the dose gradient is steep enough that accuracy of measurement may be lowered. Accordingly, we performed dosimetry using MOSFET dosimeters in pairs. We hope to increase accuracy by further increasing the number of dosimeters used simultaneously. We believe that in vivo dosimetry is a useful and necessary means of measurement in ensuring QA in external beam radiation therapy. In addition, our method enables target dose estimation in the isocenter without affecting the radiotherapy beam.

5. Conclusion

Evaluation of performance of MOSFET dosimeter revealed that angle dependence exhibited the largest coefficient of variation, of approximately 3.4%. The target dose can be estimated from the surface dose on the exit side by compensating for insufficient backscatter on the exit side by BSF. Accuracy of target dose estimation based on in vivo dosimetry with the phantom at the mean dose of two MOSFET dosimeters showed the maximum relative error of -2.8% for 20-cm-thick laminated solid tough water phantom and -6.1% for the oval water equivalent phantom.

Appendix A Relationship between phantom scattering coefficient (S_p), maximum depth dose (D_0), and in-air water collision kerma (K_r)

As shown in Fig. 10, we assume that the dose in the irradiation field of 10 × 10 cm^2 at the maximum depth (d_{max}) is D_r and the in-air water collision kerma at that dose point is K_r. We then assume that the maximum depth dose in a given irradiation field (A_T) is D_0. However, we also assume that the in-air water collision kerma K_r is constant even if the irradiation field changes (i. e. that the collimator scattering coefficient (S_c) always equals 1). Under these conditions, the relationship between K_r, D_r, and D_0 can be expressed as follows:

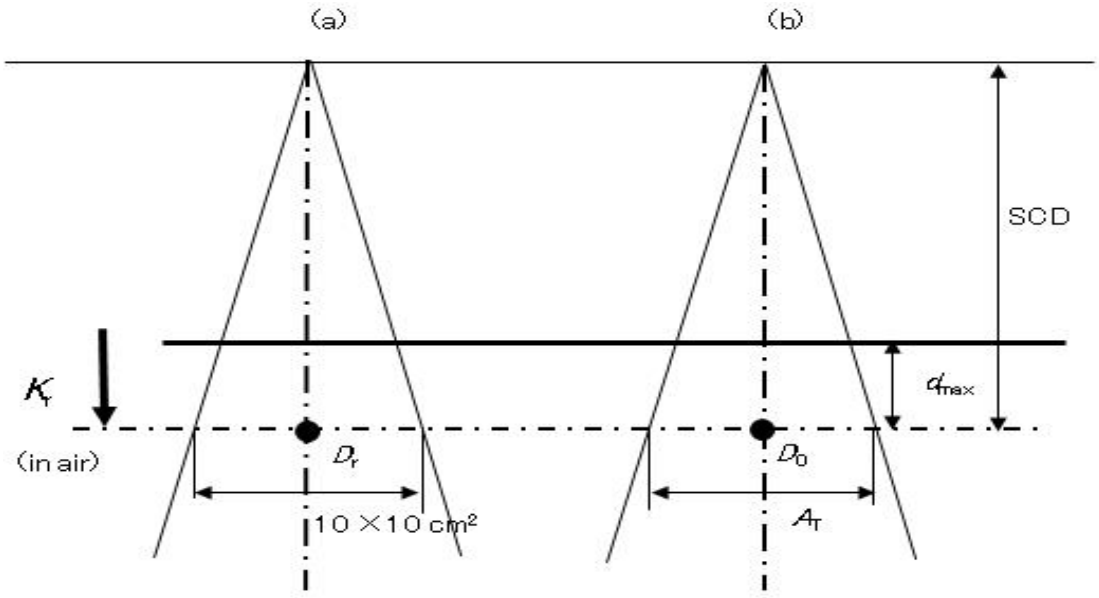

Fig. 10 (a) indicates the maximum depth dose (D_r) in the irradiation field of 10 × 10 cm^2 at the in-air water collision kerma (K_r). (b) indicates the maximum depth dose (D_0) in the irradiation field (A_T) at the in-air water collision kerma (Kr). These relationships are expressed in Equations (9) to (11).

$$S_p(A_T) = \frac{D_0}{D_r} \quad \cdots\cdots\cdots\cdots (9)$$

$$D_r = f \cdot K_r \cdots\cdots\cdots\cdots\cdots (10)$$

where S_p is a phantom scattering coefficient. The constant f is therefore expressed as:

$$f = \frac{D_0}{K_r \bullet S_p(A_T)} \cdots\cdots\cdots\cdots\cdots\cdots (11)$$

Reference

1) AAPM: Diode in vivo dosimetry for patients receiving external beam radiation therapy. AAPM Task Group #62 radiation therapy committee (February, 2005).
2) Jan V D, Ginette M: Methods for in vivo dosimetry in external radiotherapy. ESTRO physics for clinical radiotherapy booklet No1 (1994).
3) Dominique H, Ria B, Jan V, et al: Practical guidelines for the implementation of in vivo dosimetry with diodes in external radiotherapy with photon beams (Entrance Dose). ESTRO physics for clinical radiotherapy booklet No 5, (2001).
4) Hiroyuki N, Naoki S, Osamu N: Evaluation of Performance of Metal Oxide-silicon Semiconductor Field Effect Transistor (MOSFET) Dosimeter. Jpn J Radio Technol. 57(2), 234-241, (2000) (in Japanese).

5) Jason Mortom: Clinical implementation of MOSFETs for entrance dose in-vivo dosimetry with high energy photons for external beam radiation therapy. School of Chemistry and Physics University of Adelaide, (2006).
6) Bulinski K, Kukolowicz P: Characteristics of the Metal Oxide Semiconductor Field Effect Transistors for Application in Radiotherapy. Pol J Med Phys Eng, 10(1) 13-24.(2004).
7) Ramaseshan R, Kohli KS, Zhang TJ, et al: Performance characteristics of a microMOSFET as an in vivo dosimeter in radiation therapy. Phys Med Biol.49,4031-48,(2004).